Chemical Engineering Journal 386 (2020) 123917

Contents lists available at ScienceDirect

Chemical Engineering Journal

journal homepage: www.elsevier.com/locate/cej

Enhanced thermoelectric performance through optimizing structure of anionic framework in AgCuTe-based materials

Weiming Zhu[a], Zhongyuan Huang[a], Mihai Chu[a], Shuankui Li[a], Yihua Zhang[b], Weiqin Ao[b], Rui Wang[a], Jun Luo[c], Fusheng Liu[b,*], Yinguo Xiao[a,*], Feng Pan[a,*]

[a] School of Advanced Materials, Peking University, Shenzhen Graduate School, Shenzhen 518055, China
[b] College of Materials Science and Engineering, Shenzhen Key Laboratory of Special Functional Materials, Shenzhen University, Shenzhen 518060, China
[c] School of Materials Science and Engineering, Shanghai University, Shanghai 200444, China

HIGHLIGHTS

- The Se^{2-} enrichment in Te^{2-} framework is realized in AgCuTe superionic conductor.
- The Se^{2-}-rich anionic framework largely reduces the carrier concentration.
- The carrier thermal conductivity of Se^{2-}-rich samples is decreased significantly.
- A maximum ZT value of 1.2 is obtained by introducing Se^{2-} enrichment in AgCuTe sample.

GRAPHICAL ABSTRACT

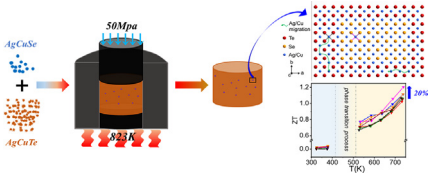

ARTICLE INFO

Keywords:
AgCuTe
Superionic conductor materials
Thermoelectrics
Defects engineering
Optimizing the anionic framework

ABSTRACT

Defects engineering is an effective approach to improve thermoelectric performance of thermoelectric materials. In this work, a simple strategy has been developed to introduce large scale defects of Se^{2-} enrichment in the Te^{2-}-based anionic framework of AgCuTe-based thermoelectric materials. As a consequence, the structure of anionic Se^{2-}/Te^{2-}-based framework is modified and its electrical transport properties are largely affected. It is observed that the carrier concentration is reduced because the Se^{2-} enrichment hinders the formation of cation vacancies, leading to the decreasing of electric conductivity and the increasing of Seebeck coefficient in high temperature range. Significantly, the electron thermal conductivity decreases to an extremely low level due to the further reduction in carrier concentration. As a result, the Se-rich AgCuTe sample achieves a maximum ZT value of 1.2 at 723 K, which is about 20% higher than that of the pristine AgCuTe sample. The results evidence that optimizing the anionic framework is an effective approach to improve the thermoelectric properties of AgCuTe and is expected to be a universal modification strategy to enhance the thermoelectric performance of other Ag/Cu-based superionic conductor materials.

1. Introduction

Thermoelectric materials, which are capable of directly converting waste heat into useful electricity, possess great potential applications in the field of waste heat recovery and environmentally-friendly refrigeration [1,2]. Generally, the performance of thermoelectric materials is evaluated by the value of a dimensionless thermoelectric figure of merit (ZT), which is defined as$ZT = S^2\sigma T/k$, where S is the Seebeck coefficient, σ is the electric conductivity, k is the thermal conductivity and T is the Kelvin temperature [3]. To obtain a high ZT value, the thermoelectric materials are required to exhibit both low k and high power factor ($PF = S^2\sigma$) simultaneously [4,5]. However, it is

* Corresponding authors.
E-mail addresses: fsliu@szu.edu.cn (F. Liu), y.xiao@pku.edu.cn (Y. Xiao), panfeng@pkusz.edu.cn (F. Pan).

https://doi.org/10.1016/j.cej.2019.123917
Received 7 October 2019; Received in revised form 17 November 2019; Accepted 21 December 2019
Available online 23 December 2019
1385-8947/

rather challenging to achieve high *ZT* value because all these essential parameters (S, σ, k) are closely coupled with each other via carrier concentration particularly. Hence, to modify one of the parameters in *ZT* formula often leads to non-cooperative changes in other parameters [6], which largely limits the improvement of thermoelectric performance and extensive applications of thermoelectric devices.

The concept of 'phonon-glass electron-crystal' (PGEC) proposed by Slack et al. is considered as an important criterion to search and seize high-performance thermoelectric materials [7]. According to the PGEC concept, high-performance thermoelectric materials should possess not only low thermal conductivity like glass but also high electric conductivity like well-ordered crystal. A series of high-performance thermoelectric materials such as clathrates [8], filled skutterudites [9] and zintl phases [10] conformed to the PGEC concept have been studied extensively. Recently, a new class of $(Ag, Cu)_2X$-based (X = S, Se, Te) superionic conductors that exhibit excellent thermoelectric properties have been reported [11,12], and the new concept 'phonon-liquid electron-crystal' (PLEC) developed on the basis of the PGEC concept has been proposed to explain the structural properties of such superionic conductors [13]. These $(Ag, Cu)_2X$-based (X = S, Se, Te) superionic conductors could transform into the rock-salt-type structure at high temperature, in which the anions atoms form rigid crystalline sublattice and the cations surrounding the anions form liquid-like sublattice [14,15]. The ultra-low intrinsic thermal conductivity (k) can be achieved due to the disorder and flow of cations in the liquid-like sublattice, while the rigid crystalline sublattice of anions provides a good electrical transport channel, enabling these compounds to achieve high thermoelectric properties [15]. A variety of $(Ag, Cu)_2X$-based (X = S, Se, Te) superionic conductors with low intrinsic k less than 1 $W{\cdot}m^{-1}{\cdot}K^{-1}$ and high *ZT* value more than 1.5 have been reported, such as Cu_2S, Cu_2Se, Ag_2Se, AgCuSe [13,16–18], indicating that these compounds are potential candidates in practical application as thermoelectric materials.

Among all $(Ag, Cu)_2X$-based compounds, ternary compounds AgCuX (X = S, Se, Te) exhibit special characteristics in thermoelectric and structural properties. A peak *ZT* of 0.95 at 673 K in AgCuSe has been reported [19], which is significantly higher than those binary compounds, suggesting that the ternary compounds AgCuX are valuable thermoelectric materials in the medium-high temperature range. In medium-high temperature range, the ternary compounds possess rock-salt-type structure, in which Ag^+/Cu^+ cations could randomly diffuse within the VII-based (VII = S^{2-}, Se^{2-}, Te^{2-}) anionic rigid sublattice [18].

In 2018, Roychowdhury et al. reported that a high *ZT* value of 1.2 at 723 K can be achieved in a new superionic conductor AgCuTe [20] because its soft phonon modes lead to ultralow thermal conductivity. Furthermore, the modification of the composition of cations and anions can be realized to improve the thermoelectric performance of the AgCuTe compound [20,21]. These works demonstrate that AgCuTe is a novel ternary compound that held excellent thermoelectric properties in medium-high temperature range (500 ~ 800 K). Naturely, the AgCuTe-based materials have attracted our attention and we are motivated to further improve their thermoelectric performance through utilizing new strategies.

In this work, we have developed an effective strategy to optimize the anionic framework of AgCuTe thermoelectric compound by introducing the large scale defects of Se^{2-} enrichment in the Te^{2-}-based anionic framework. Specifically, a series of different proportions of AgCuTe and AgCuSe powders are mixed and then dispersed, dried and hot-pressed to obtain bulk samples, and the structural characterization results show that the Se^{2-} enrichment is introduced to the Te^{2-}-based anionic framework. The Se^{2-} enrichment in the Te^{2-}-based anionic framework significantly affects the carrier concentration of the Se-rich samples, thus successfully lead to the optimization of the electrical transport properties and reduction of the thermal conductivity. As a result, a maximum *ZT* value of 1.2 is obtained for AgCuTe with 8 wt% AgCuSe sample at 723 K, realizing a 20% enhancement in *ZT* value compared to the pristine AgCuTe sample.

2. Experimental section

2.1. Materials

Cu powder (99.99%), Te powder (99.99%), Se powder (99.99%) and $AgNO_3$ (99.9%) were purchased from Aladdin Industrial Corporation, Ag powder (99.99%). $NaBH_4$ (99%), $Cu(NO_3)_2{\cdot}3H_2O$ (99.9%) were purchased from Sinopharm Chemical Reagent Co., Ltd. All the chemicals were used without further purification.

2.2. Synthesis of AgCuTe powder and AgCuSe powder

AgCuTe powder were prepared through a solid melting reaction. The Ag, Cu and Te powders were weighted according to the stoichiometric ratio, then these three kinds of powders were uniformly mixed and put into a carefully cleaned quartz tube. The quartz tube was sealed under a vacuum of 10^{-3} Pa using the Partulab MRVS Vacuum Sealing System, then was slowly heated to 1323 K in 24 h, annealed for 24 h and then slowly cooled down to room temperature in 24 h in a muffle furnace. The obtained ingot was ground in an Argon filled glove box for 1 h to obtain fine powders.

AgCuSe powder was synthesized using the aqueous methods as reported by Han et al [22]. Se powder and $NaBH_4$ caplets were dispersed in distilled water in a beaker and stirred for 25 min at room temperature to form a colorless selenium precursor solution. $AgNO_3$ and $Cu(NO_3)_2{\cdot}3H_2O$ were dissolved in distilled water in another beaker, and then quickly added into the Se-precursor solution to generate black precipitates. The precipitates were collected by filtration, successively washed 4 times with distilled water and dried in a vacuum drying oven at 70 °C for 24 h.

2.3. Synthesis of AgCuTe/x wt% AgCuSe bulk samples

The synthesized AgCuTe and AgCuSe powders were weighed according to different mass ratios and mixed. Then the as-mixed powder was added into 100 ml absolute ethanol. After sonicate and stirring for 30 min, the precipitations were collected and dried at 70 °C for 24 h to obtain the mixed powder. AgCuTe/x wt% AgCuSe (x = 0, 2, 4, 6, 8, 10, 12) bulk samples were obtained by hot pressing the as-mixed powder into a cylinder using a φ10 mm graphite die at 823 K for 50 min under the uniaxial stress of 50 MPa and then were annealed at 773 K for three weeks afterward to ensure the achievement of thermodynamic equilibrium. The obtained bulk samples were labeled as S-x (x = 0, 2, 4, 6, 8, 10, 12) samples.

2.4. Characterization

The X-ray diffraction (XRD) data were collected on a Bruker D8 Advance powder X-ray diffractometer with a Cu-Kα radiation (λ = 1.5406 Å). The sample morphologies were measured by field emission scanning electron microscopy (SEM) on a Zeiss SUPRA-55. The backscattered electron (BSE) images of polished surfaces and energy dispersive X-ray analysis (EDS) images were collected by a FIB microscope (FEI Scios).

2.5. Thermoelectric measurements

The temperature-dependent Hall coefficients (R_H) were measured using the van der Pauw technique under a reversible magnetic field of 1.5 T. The temperature-dependent carrier concentration (n) and mobility (μ) were calculated using $n = 1/(eR_H)$ and $\mu = \sigma R_H$, respectively. The Seebeck coefficients (S) and electric resistivity (r) were simultaneously measured under a helium atmosphere using a thermoelectric

measurement system (ZEM-3, ULVAC-RIKO, Japan) within the temperature from 300 K to 723 K. The electric conductivity (σ) is calculated from the measured data of electric resistivity, where $\sigma = 1/r$. The thermal conductivity (κ) was calculated through $\kappa = D\rho C_p$, where D, ρ and C_p are the thermal diffusivity coefficient, density and specific heat capacity. The thermal diffusivity coefficient was obtained by measuring pellets with a diameter of 10 mm and thickness of 1 mm using a Netzsch LFA 457 from 300 K to 723 K. The C_p is calculated by adopting the Dulong-Petit Law and the densities of the pellets were determined using the Archimedes method. Please refer to the Supplementary material for detailed calculation process.

3. Results and discussion

A series of samples labeled S-x (x = 0, 2, 4, 6, 8, 12) were firstly obtained by hot pressing the as-mixed AgCuTe with x wt% AgCuSe powder. As-prepared bulk samples were annealed at 773 K for three weeks afterward to ensure the achievement of thermodynamic equilibrium. According to the previous report, AgCuTe undergoes multiple phase transitions in the temperature range from 400 K to 500 K, and its thermoelectric properties are prominent above 500 K associated with the rock-salt-type structural phase [20,21]. To investigate and clarify the relationship between the thermoelectric properties and the structural properties of AgCuTe at high temperature in detail, we performed XRD measurements of the pristine S-0 sample at different temperatures in the range of 303 to 723 K. As demonstrated in Fig. 1(a), the XRD patterns vary gradually during the warming process from 303 K to 723 K, which clearly demonstrates the occurrence of structural phase transition, i.e. the sample transforms into the rock-salt-type structural phase above the temperature of 523 K. Moreover, Fig. S1 shows the temperature dependent XRD patterns of the pristine S-0 sample during the cooling process, which indicated that the phase transition of AgCuTe is reversible. The XRD refinement pattern of the pristine S-0 sample at 723 K is shown in Fig. 1(b), the observed XRD pattern can be well fitted with the rock-salt-type structural model, which represents a typical structure of Ag/Cu-based superionic conductors [23], the illustration of crystal structure for high temperature rock-salt-type phase of AgCuTe is shown in Fig. 1(e), in which Ag^+/Cu^+ cations could randomly diffuse within the Te-based anionic framework of cubic sublattice. In contrast, the pristine S-0 sample is observed to be multiphase at 303 K as revealed by the XRD pattern in Fig. 1(c). Beside of the diffraction peaks originated from $Cu_{0.8}Ag_{0.96}Te$ (JCPDS 78-0497, similar) phase, the peaks that come from both Cu_2Te (JCPDS 40-1325) and Ag_2Te (JCPDS 81-1985) are also observed in the XRD pattern. The complicated XRD pattern at 303 K confirms that the as-prepared sample contains multiple phases at room temperature, which is consistent with previous reports [21]. Furthermore, the backscattered electron (BSE) image and energy dispersive X-ray analysis (EDS) mapping images of polished surface of the pristine S-0 sample are shown in Fig. 1(d), which also demonstrates the complex composition of the pristine S-0 at 303 K.

As described previously, a series of samples labeled as S-x are obtained by introducing Se enrichment into AgCuTe. In order to study the structural evolution of the Se-rich samples, the temperature dependence of XRD patterns of the Se-rich S-8 sample is collected and shown

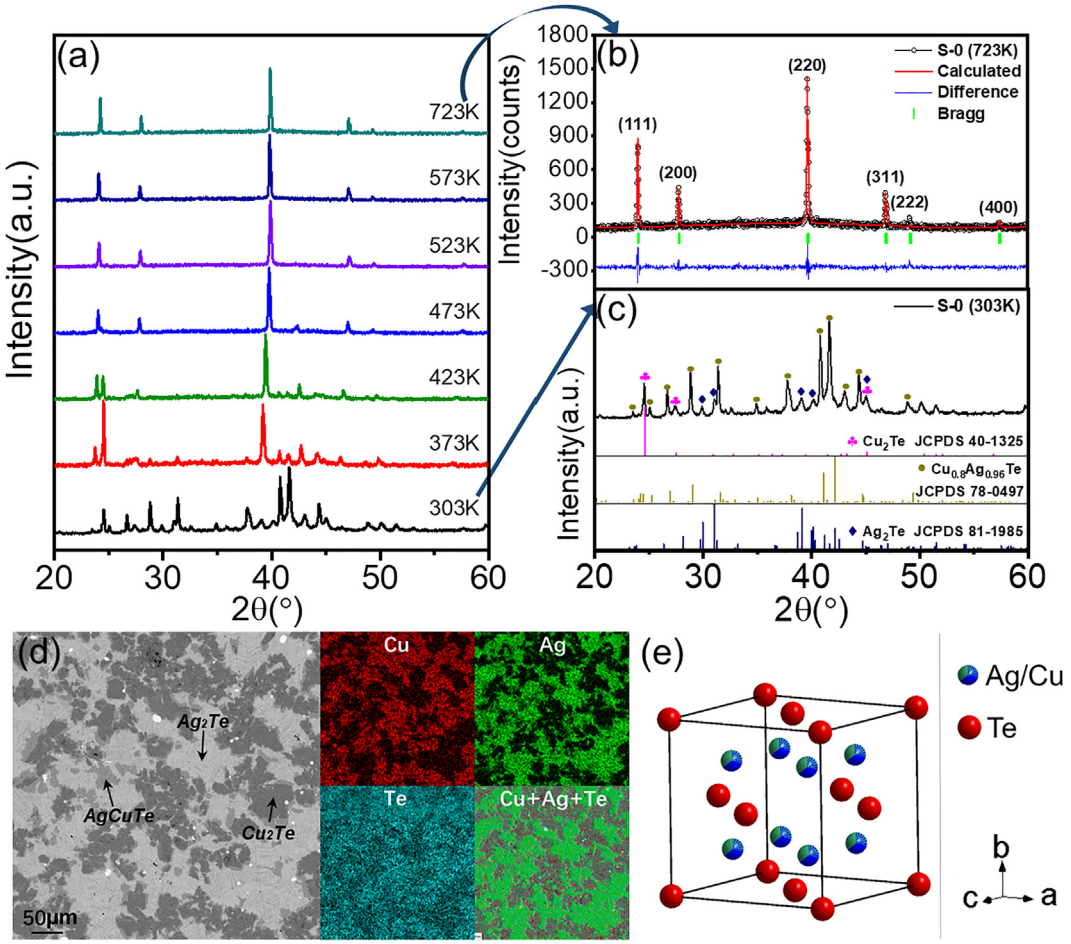

Fig. 1. (a) Temperature dependence of XRD patterns of the pristine S-0 sample. (b) XRD refinement pattern of the pristine S-0 sample at high temperature of 723 K; (c) XRD pattern of the pristine S-0 sample at 303 K. (d) Backscattered electron image and EDS mapping images of the pristine S-0 sample; (e) Crystal structure of the high temperature phase of AgCuTe.

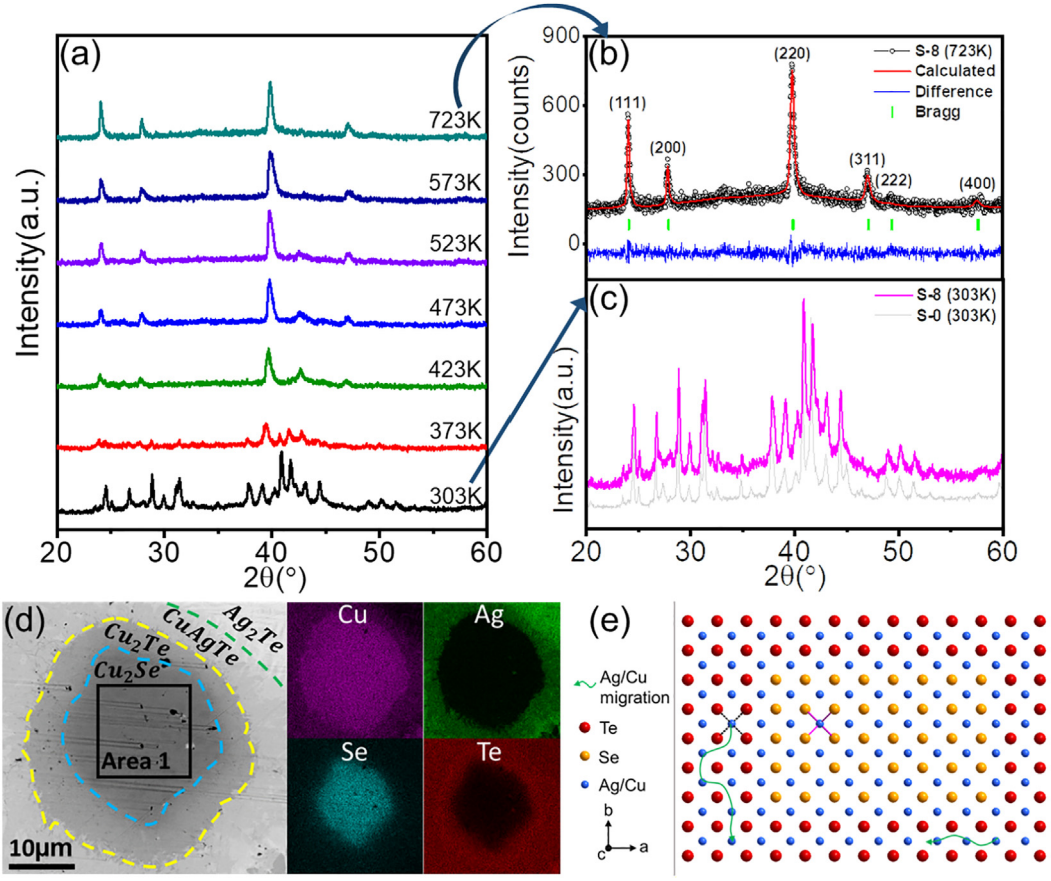

Fig. 2. (a) Temperature dependence of XRD patterns of the Se-rich S-8 sample. (b) XRD refinement pattern of the Se-rich S-8 sample at high temperature of 723 K; (c) XRD pattern of the Se-rich S-8 sample at 303 K. (d) Backscattered electron image and EDS mapping images of the Se-rich S-8 sample; (e) Schematic illustration demonstrates the Se^{2-} enrichment in the Te^{2-}-based framework and the free migration of Ag^{+}/Cu^{+} cations.

in Fig. 2(a). For comparison, the XRD patterns for both the pristine S-0 sample and the Se-rich S-8 sample are measured under the same measurement conditions. During the heating process, the Se-rich S-8 sample also undergoes a phase transition similar to the pristine S-0 sample, and finally transforms into the rock-salt-type structural phase above temperature of 523 K. However, it is noticed that the peaks width broaden significantly in the XRD patterns of the Se-rich S-8 sample compared to that in the pristine S-0 sample, suggesting the reduction of orderliness and the formation of structural cluster in Se^{2}-rich Te^{2-}-based framework.

As shown in Fig. 2(b), the Se-rich S-8 sample possesses the same structure as the pristine S-0 sample at 723 K, but the peak intensity decreases significantly and the diffuse background increases largely in the Se-rich S-8 sample compared to that in pristine S-0 sample, which is attributed to the formation of structural cluster in the Se^{2}-rich Te^{2-}-based framework. The deduced structural parameters of these two samples are given in Table S1. It is shown that the *a*-axis of the Se-rich S-8 sample is 6.3992 Å, which is smaller than that of the pristine S-0 sample (6.4247 Å). The shrinkage of the lattice is attributed to the incorporation of Se^{2-} anion with smaller ionic radius in the Te^{2-}-based framework [24].

Indeed, the segregation of the Se^{2-} enrichment in the Te^{2-}-based framework can be reflected by the results of microstructural analysis. As shown in Fig. 2(d) and Fig. S2, the BSE image and EDS mapping images of polished surface of the Se-rich S-8 sample reveal that the Se element is significantly enriched after cooling down from high-temperature superionic conducting state. Despite the evolution of phase structure at different temperatures, the rigid anion framework is supposed to be maintained as reported in many works [12,19,25]. Therefore, it is fairly to assume that Se^{2-} anion is enriched in the Se-contained samples in both high temperature and low temperature phases, while the cations, i.e. Ag^{+} cation and Cu^{+} cation can still migrate freely. These results are different from the report in reference [20], in which the authors claimed that Se is alloying at the Te site to form $AgCuTe_{1-x}Se_{x}$ (x = 0, 0.10, 0.15) solid solution. The schematic illustration of the structural detail of the Se-rich samples is shown in Fig. 2(e), which demonstrates the Se^{2-} enrichment in the Te^{2-}-based framework.

The XRD pattern of the Se-rich S-8 sample at 303 K is shown in Fig. 2(c), which is very similar to the XRD pattern of the pristine S-8 sample at 303 K, indicating that the Se-rich S-8 sample has a similar complex multiphase structure at room temperature. In order to further determine the composition of the compound containing Se, the microstructural analysis is performed and quantitative EDS result of the Area 1 in Fig. 2(c) is listed in Table S2. According to the quantitative EDS microanalysis results, the Se enrichment area in the Se-rich S-8 sample is generated in the form of Cu_2Se at room temperature. The appearance of Cu_2Se phase can be understood in the framework of superionic conductor. Given the fact that the Te^{2-}-based framework has larger tetrahedral interstices than the Se^{2-}-based framework, Ag^{+} cation is more likely to migrate into the tetrahedral interstices of Te^{2-}-based framework and Cu^{+} cation is more likely to migrate into the tetrahedral interstices of Se^{2-}-based framework. Thereby Ag^{+} and Cu^{+} cations are redistributed to form Cu_2Se and the core-shell structure of Fig. 2(d) at room temperature.

The Se^{2-} enrichment in the Te^{2-}-based framework significantly affects the electrical transport properties of the system. As shown in Fig. 3(a), compared with the pristine S-0 sample, the Se-rich samples exhibit relatively lower electric conductivity over the whole

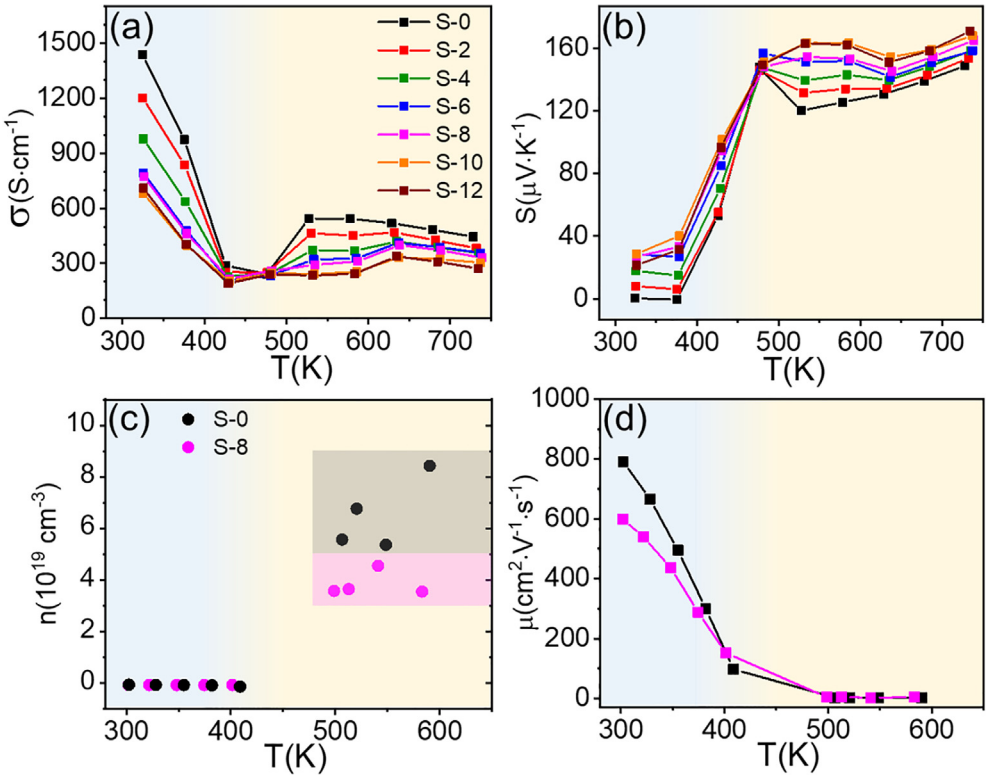

Fig. 3. (a, b) Temperature dependence of electric conductivity (σ), Seebeck coefficient (S) of all samples. (c, d) Temperature dependence of carrier concentration (n) and mobility (μ) of the pristine S-0 sample and the Se-rich S-8 sample.

temperature range, and electric conductivity gradually decreases with increasing Se content. To understand the influence of Se^{2-} enrichment in the Te^{2-}-based framework on the electric transportation, we studied the variation of carrier concentration (n) and mobility (μ) as a function of temperature in the pristine S-0 sample and the Se-rich S-8 sample, respectively. It is known that the conductivity of the system is mainly determined by the carrier concentration in the high temperature rock-salt-type structure (> 523 K). As shown in Fig. 3(c) and (d), the carrier concentration reduced apparently from (5 ~ 9) × 10^{19} cm^{-3} in the pristine S-0 sample to (3 ~ 5) × 10^{19} cm^{-3} in the Se-rich S-8 sample, which indicates significant reduction in electric conductivity. The decrease of carrier concentration can be attributed to the reduction of Cu/Ag vacancies since the bond energy of Ag-Se/Cu-Se is larger than that of Ag-Te/Cu-Te [20].

The variation of Seebeck coefficients (S) as a function of temperature for all investigated samples are shown in Fig. 3(b). It is obvious that all samples exhibit positive S due to intrinsic Cu and Ag vacancies. Because the samples possess the rock-salt structure above 523 K, high band degeneracy is achieved due to the highly symmetrical crystal structure [26], resulting in high Seebeck coefficients for all the samples. The Se-rich samples possess a higher Seebeck coefficient than that of the pristine S-0 sample, which is associated with the lower carrier concentration. Moreover, the energy filtering effect also contributes to the improvement of the Seebeck coefficient [27]. As described above, the Se-rich samples form a core-shell structure at room temperature, which forms a series of energy barriers at the boundaries of phases, thereby filtering the lower energy carriers that are harmful to the Seebeck coefficient, hence the Seebeck coefficient of the Se-rich samples near room temperature increase significantly with the increase of Se content. Meanwhile, the power factor of the Se-rich samples that shown in Fig. 4(c) is slightly improved near the room temperature, which is also the embodiment of the energy filtering effect. The core-shell structure disappears and the sample crystalizes in rock-salt-type structure at high temperature, which can be clearly seen from the XRD results in Fig. 2(b). Therefore, the improvement of the Seebeck coefficient of the Se-rich samples at high temperature is mainly attributed to the decrease in carrier concentration. As a result, the Seebeck coefficient is increased from 149 μV/K of the pristine S-0 sample to 171 μV/K of the Se-rich S-12 sample at 723 K.

As mentioned above, AgCuTe is composed of relatively rigid Te^{2-}-based framework and "liquid-like" Ag^{+}/Cu^{+} cation-mixed substructure. In this scenario, Ag^{+}/Cu^{+} cations are vibrations around the equilibrium position, resulting in extremely strong phonon scattering. As shown in Fig. 4(a), the vibrations of Ag^{+}/Cu^{+} cations push the mean free path of the phonons to approach the solid limit, which leads to extremely low thermal conductivity in the pristine S-0 sample about 0.5 ~ 0.7 W/(m·K) at high temperature. The Se^{2-} enrichment in the Te^{2-}-based framework also has a significant influence in the thermal conductivity of the samples. As shown in Fig. 4(a), the Se-rich samples achieve a maximum reduction of 20% in thermal conductivity at 723 K, i.e. from 0.68 $W{\cdot}m^{-1}{\cdot}K^{-1}$ of the pristine S-0 sample to 0.54 $W{\cdot}m^{-1}{\cdot}K^{-1}$ of the Se-rich S-12 sample. The significant decrease in thermal conductivity is attributed mainly to the large decrease in carrier thermal conductivity. Fig. 4(b) shows the temperature dependence of carrier thermal conductivity(κ_e) which is calculated according to the Wiedemann-Franz law ($\kappa_e = \sigma LT$), where L is the Lorenz number and it is estimated by using the SPB model [28]. Since the electric conductivity of all samples decreases with increasing Se concentration, the carrier thermal conductivity reduces from 0.57 $W{\cdot}m^{-1}{\cdot}K^{-1}$ in the pristine S-0 sample to 0.34 $W{\cdot}m^{-1}{\cdot}K^{-1}$ in the Se-rich S-12 sample at 723 K.

Fig. 4(c) exhibits the calculated temperature-dependent thermoelectric power factor ($S^2\sigma$), which is comparable to the power factor as reported in AgCuTe compound in high-temperature range [21]. The temperature-dependent figure of merit (ZT) of all samples is shown in Fig. 4(d). The ZT value of the pristine S-0 sample increases with temperature and reaches 1.0 at 723 K. Due to the reduced thermal conductivity and maintained high power factor, a highest ZT value of 1.2 at 723 K for the Se-rich S-8 sample is achieved, which is nearly 20%

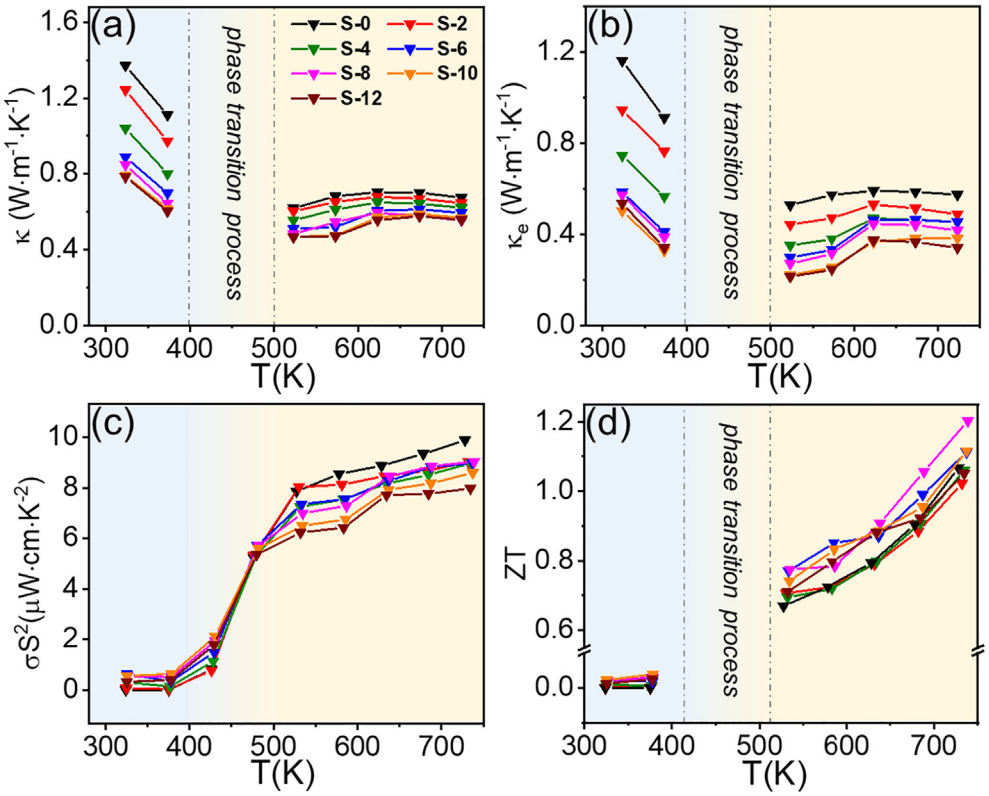

Fig. 4. (a–d) Temperature dependent total thermal conductivity (κ), carrier thermal conductivity (κ_e), power factor ($S^2\sigma$) and figure of merit (ZT) of all samples.

enhancement compared to that of the pristine S-0 sample, indicating that the Se^{2-} enrichment in the Te^{2-}-based framework is a facile and effective approach to improve the thermoelectric properties of AgCuTe.

4. Conclusion

In summary, by introducing Se-enrichment in the Te^{2-}-based framework of AgCuTe superionic conductor, the thermoelectric performance is improved largely. As a result, the Se-rich S-8 sample reaches the highest ZT value of 1.2 at 723 K, achieving an approximate 20% improvement over the pristine S-0 sample. It is assumed that the Se^{2-} enrichment in the Te^{2-}-based framework hinders the formation of cation vacancies in the rock-salt structural phase due to larger bond energy between Se^{2-} anion and Ag^{+}/Cu^{+} cations, as a consequence, the carrier concentration of Se-rich samples is significantly reduced. The electric conductivity decreases accompanied by the increase in Seebeck coefficient, resulting in the maintains of power factor at high-temperature. The decrease of electric conductivity also leads to the decrease of the carrier thermal conductivity, thereby the thermal conductivity of the Se-rich samples is reduced significantly.

Declaration of Competing Interest

The authors declare that they have no known competing financial interests or personal relationships that could have appeared to influence the work reported in this paper.

Acknowledgements

The work was financially supported by Soft Science Research Project of Guangdong Province (No. 2017B030301013), Shenzhen Science and Technology Research Grant (ZDSYS201707281026184) and Guangdong Basic and Applied Basic Research Foundation (2019A1515010832).

Appendix A. Supplementary data

Supplementary data to this article can be found online at https://doi.org/10.1016/j.cej.2019.123917.

References

[1] A.J. Minnich, M.S. Dresselhaus, Z.F. Ren, G. Chen, Bulk nanostructured thermoelectric materials: current research and future prospects, Energy Environ. Sci. 2 (2009) 466–479.
[2] I. Petsagkourakis, K. Tybrandt, X. Crispin, I. Ohkubo, N. Satoh, T. Mori, Thermoelectric materials and applications for energy harvesting power generation, Sci. Technol. Adv. Mater. 19 (2018) 836–862.
[3] J. He, T.M. Tritt, Advances in thermoelectric materials research: looking back and moving forward, Science 357 (2017) 6358.
[4] Y.Z. Pei, H. Wang, G.J. Snyder, Band engineering of thermoelectric materials, Adv. Mater. 24 (2012) 6125–6135.
[5] G.J. Tan, L.D. Zhao, M.G. Kanatzidis, Rationally designing high-performance bulk thermoelectric materials, Chem. Rev. 116 (2016) 12123–12149.
[6] H.J. Goldsmid, The Physics of Thermoelectric Energy Conversion, Morgan & Claypool Publishers, San Rafael, 2017, pp. 1–106.
[7] G.A. Slack, CRC Handbook of Thermoelectrics, 1995, pp. 407–440.
[8] H. Kleinke, New bulk materials for thermoelectric power generation: clathrates and complex antimonides, Chem. Mater. 22 (2010) 604–611.
[9] B.C. Sales, D. Mandrus, R.K. Williams, Filled skutterudite antimonides: a new class of thermoelectric materials, Science 272 (1996) 1325–1328.
[10] E.S. Toberer, A.F. May, G.J. Snyder, Zintl chemistry for designing high efficiency thermoelectric materials, Chem. Mater. 22 (2010) 624–634.
[11] H.L. Liu, X. Shi, F.F. Xu, L.L. Zhang, W.Q. Zhang, L.D. Chen, Q. Li, T. Day, G.J. Snyder, Copper ion liquid-like thermoelectrics, Nat. Mater. 11 (2012) 422–425.
[12] P.F. Qiu, X. Shi, L.D. Chen, Cu-based thermoelectric materials, Energy Storage Mater. 3 (2016) 85–97.
[13] Y. He, T. Day, T.S. Zhang, H.L. Liu, X. Shi, L.D. Chen, G.J. Snyder, High thermoelectric performance in non-toxic earth-abundant copper sulfide, Adv. Mater. 26 (2014) 3974–3978.
[14] S.A. Danilkin, M. Avdeev, M. Sale, T. Sakuma, Neutron scattering study of ionic diffusion in Cu–Se superionic compounds, Solid State Ionics 225 (2012) 190–193.
[15] T.A. Miller, J.S. Wittenberg, H. Wen, S. Connor, Y. Cui, A.M. Lindenberg, The mechanism of ultrafast structural switching in superionic copper (I) sulphide nanocrystals, Nat. Commun. 4 (2013) 1369.
[16] B. Yu, W.S. Liu, S. Chen, H. Wang, H.Z. Wang, G. Chen, Z.F. Ren, Thermoelectric properties of copper selenide with ordered selenium layer and disordered copper layer, Nano Energy 1 (2012) 472–478.

[17] W.L. Mi, P.F. Qiu, T.S. Zhang, Y.H. Lv, X. Shi, L.D. Chen, Thermoelectric transport of Se-rich Ag_2Se in normal phases and phase transitions, Appl. Phys. Lett. 104 (2014) 133903.
[18] J.Y. Zhang, J.H. Zhu, L. You, K. Guo, Z.L. Lia, W.G. Lin, J. Huang, J. Luo, Enhanced and stabilized n-type thermoelectric performance in α-CuAgSe by Ni doping, Mater. Today Phys. 10 (2019) 100095.
[19] A.J. Hong, T. Li, H.X. Zhu, X.H. Zhou, Q.Y. He, W.S. Liu, Z.B. Yan, J.M. Liu, Z.F. Ren, Anomalous transport and thermoelectric performances of CuAgSe compounds, Solid State Ionics 261 (2014) 21–25.
[20] S. Roychowdhury, M.J. Jana, J. Pan, S.N. Guin, D. Sanyal, U.V. Waghmare, K. Biswas, Soft phonon modes leading to ultralow thermal conductivity and high thermoelectric performance in AgCuTe, Angew. Chem. Int. Ed. Engl. 57 (2018) 4043–4047.
[21] R.N. Wu, Z.L. Li, Y.B. Li, L. You, P.F. Luo, J. Yang, J. Luo, Synergistic optimization of thermoelectric performance in p-type Ag_2Te through Cu substitution, J. Materiomics (2019).
[22] C. Han, Q. Sun, Z.X. Cheng, J.L. Wang, Z. Li, G.Q. Lu, S.X. Dou, Ambient scalable synthesis of surfactant-free thermoelectric CuAgSe nanoparticles with reversible metallic-n-p conductivity transition, J. Am. Chem. Soc. 136 (2014) 17626–17633.
[23] K.P. Zhao, P.F. Qiu, X. Shi, L.D. Chen, Recent advances in liquid-like thermoelectric materials, Adv. Funct. Mater. 1903867 (2019).
[24] Y. Yao, B.P. Zhang, J. Pei, Y.C. Liu, J.F. Li, Thermoelectric performance enhancement of Cu_2S by Se doping leading to a simultaneous power factor increase and thermal conductivity reduction, J. Mater. Chem. C 5 (2017) 7845–7852.
[25] P.F. Qiu, M.T. Agne, Y.Y. Liu, Y.Q. Zhu, H.Y. Chen, T. Mao, J. Yang, W.Q. Zhang, S.M. Haile, W.G. Zeier, J. Janek, C. Uher, X. Shi, L.D. Chen, G.J. Snyder, Suppression of atom motion and metal deposition in mixed ionic electronic conductors, Nat. Commun. 9 (2018) 2910.
[26] J.W. Zhang, L.R. Song, S.H. Pedersen, H. Yin, L.T. Hung, B.B. Iversen, Discovery of high-performance low-cost n-type Mg_3Sb_2-based thermoelectric materials with multi-valley conduction bands, Nat. Commun. 7 (2017) 13901.
[27] Y.C. Zhang, G.D. Stucky, Heterostructured approaches to efficient thermoelectric materials, Chem. Mater. 26 (2014) 837–848.
[28] H.S. Kim, Z.M. Gibbs, Y. Tang, H. Wang, G.J. Snyder, Characterization of Lorenz number with Seebeck coefficient measurement, APL Mater. 3 (2015) 041506.